Jurnal Tribologi 31 (2021) 115-129

MYTRIBOS Malaysian Tribology Society

Jurnal Tribologi

Website : jurnaltribologi.mytribos.org e-issn: 2289-7232

A comparative study on wear behavior of AZ91D Mg alloy in dry and simulated body fluid for bio-implant materials

Satpal Kundu, Lalit Thakur *

Mechanical Engineering, National Institute of Technology, Kurukshetra, INDIA.
*Corresponding author: lalitthakur@nitkkr.ac.in

KEYWORDS

Magnesium
AZ91D
Bio-implant
Wear
Simulated body fluid

ABSTRACT

The magnesium-based AZ91D alloy is gaining popularity among researchers for temporary bio-implants, and this research article targets the in-depth sliding wear study of AZ91D material in dry and simulated body fluid. Stainless steel SS316L disc was used as the counter face against the AZ91D material specimens in pin-on-disc sliding wear experimentation. Wear rates were calculated at different sliding velocities of 0.25, 0.5, and 1 m/s, normal loads of 20, 40, and 80 N, keeping a fixed sliding distance of 2000 m. Wear maps of the investigated material were made to determine the different wear regimes and wear mechanisms. Abrasive wear occurred at a sliding velocity of 0.25 m/s and 20 N load in dry contact, whereas at 40 N in the simulated body fluid. Due to thermal softening followed by severe plastic flow, the wear was observed in both cases at a load of 80 N and sliding speed of 1 m/s. The result shows that the wear rate was increased in simulated-body fluid compared to the dry condition due to rapid corrosion of the AZ91D alloy, primarily to enhance the mass loss under high load.

1.0 INTRODUCTION

Magnesium (Mg) alloys have become attractive bio-implant materials due to their close properties to the human bone. An estimated half amount of the total physical Mg available in the human body is present in the bones (Staiger et al., 2006). Mg and its alloys occupy the benefit of bio-degradability and similar mechanical properties to natural bone. Mg alloys have remarkable advantages over the commercially available titanium, stainless steel, and Co-Cr-Ni alloy implants (Radha and Sreekanth, 2017). Mg alloy's elastic modulus is close to the human bone's elastic

Received 2 June 2021; received in revised form 29 July 2021; accepted 20 October 2021.
To cite this article: Kundu and Thakur (2021). A comparative study on wear behavior of AZ91D Mg alloy in dry and simulated body fluid for bio-implant materials. Jurnal Tribologi 31, pp.115-129.

modulus in the range of 3-20 GPa (Peron et al., 2017). Hence, the possibility of the stress shielding occurrence is minimum (Staiger et al., 2006). The composition of the porous Mg was found similar to that of bone, which is sufficient for load-bearing applications along with high inter-connectivity and mechanical properties (Kang et al., 2019). In-vivo biodegradation and biocompatibility behavior of Mg-Nd-Zn-Zr alloy coated brushite screws in dental implants were examined, and it was observed that alloy could slow down its degradation rate along with superior osteoinductivity (Kong et al., 2018). In-vivo studies after four weeks of implantation of Mg-0.5 Ca found good bio-compatibility and increased new bone formation (Makkar et al., 2018). The Mg alloys are helpful in biomedical applications due to the effects of alloying elements on bio-compatibility, corrosion resistance, and mechanical properties (Chen et al., 2019). However, many of the requirements of mechanical compatibility are not fulfilled by as-cast Mg alloys to replace the stainless steel or titanium-based bio-implants. Among the AZ series of Mg alloys, AZ91D (1% Zn and 9 % Al) has now become the most extensively explored material due to its good mechanical properties, corrosion resistance, and close properties to the human bones. Thus, it is more beneficial for making bio-implants (Ratna et al., 2016).

Apart from bio-compatibility and mechanical properties, bio-implant material's tribological behavior also decides its usage in the human body. Many authors have studied the wear behavior of AZ91D material in different operating conditions. Sathish et al. (2019) studied the sliding wear behavior of magnesium composite using the pin-on-disk apparatus. The wear behavior was analyzed using the wear maps, and the wear mechanisms were adhesion, delamination, oxidation, and thermal softening. The effect on wear rate due to SBF's induced corrosion plays a leading role, whereas the effect of SBF's lubrication was to reduce the coefficient of friction. A similar observation was found in the study of Mg-Zn-Ca alloy by other researchers (Li et al., 2016). Xiaobo et al. (2019) found that wear was significantly controlled because of $Mg(OH)_2$ and SBF lubrication, but corrosion increased because of the interaction between the alloy and wear debris. Siti et al. (2019) studied the similarities between the mechanical properties of human bone with the metallic load-bearing implants made of high wear-resistance CoCrMo based material. Xiao et al. (2018) found that the wear rate of magnesium composite rises as the normal load increases at all values of sliding speeds, and at higher loads, the plastic deformation is more significant than that at higher speeds. Kumar et al. (2017) studied the tribological study of AZ91 Mg alloy versus Al-6351 alloy using dry sliding conditions. The enhancement in the wear of alloy was attributed to the composite effect of adhesive and abrasive wear mechanisms. Imran and Lathe (2018) found that the wear rate of AZ91 Mg alloy composite is reduced at lower sliding speed and increases with an increase in the sliding speed. Ilanaganar and Anbuselvan (2018) found that in a mild wear regime of AZ31B Mg alloy, the wear increases abruptly beyond a certain critical load on gradually increasing the applied load and sliding velocity. Chelliah et al. (2017) observed that the wear rate is reduced by 6.2 times of homogenized AZ91 Mg alloy compared to as-cast AZ91 Mg alloy due to the growth of in-situ eutectic (α + β) phase, leading to the minimum wear rate in the sub-surface region. Kumar et al. (2020) found that a tribo-film is formed on large $Mg_{17}Al_{12}$ precipitates, while the α-Mg matrix mainly shows wear in AZ91 Mg alloy. Zhou et al. (2018) reported that delamination appears to be the predominant wear mechanism along with the micro-ploughing and micro-cutting during the sliding adhesive wear of AZ91D Mg alloy nanocomposite.

The present research compares the sliding wear behavior of AZ91D Mg alloy in dry and SBF solution, which is one of the promising research topics for bio-implant material. There is a scarcity of work related to the in-depth study of the wear maps and comparative wear behavior of AZ91D Mg alloy in simulated body fluid lubrication. The wear experiments were performed on pin-on-

disc testing under dry and SBF lubricated sliding conditions. Moreover, the samples were tested under different normal loads and sliding speeds to estimate the wear rates and development of wear maps. These wear maps are very useful to explain the wear behavior of any material. It helps to define the working limits (wear regimes) of any material subjected to different tribological conditions. The SEM-EDS techniques examined the microstructure and worn-out surfaces of the samples subjected under different tribological conditions (dry and SBF lubrication). The detailed examination of the SEM images of the worn-out samples has provided meaningful information about wear mechanisms in different wear regimes, which has been reported in the current manuscript.

1.0 MATERIALS AND METHODS

In the present research, the commercially available AZ91D Mg alloy sheets of 150 × 100 × 6 mm were procured from Nextgen Steel and Alloys Mumbai, India. The composition of procured annealed AZ91D Mg sheets (at 613 K) as specified by the manufacturer is given in Table 1.

Table 1: AZ91D Mg alloy's chemical composition

Al	Zn	Mn	Si	Cu	Ni	Other	Mg
8.3-9.7	0.35-1	0.15	0.1	0.03	0.002	0.02	Balance

Microstructural examination of unused and worn-out AZ91D Mg alloy samples has been done by scanning electron microscopy (SEM) attached with energy-dispersive X-ray spectroscopy (EDS) (JSM-6390 LV, Jeol Japan) and optical microscope (OM) (DeXel Imaging, Conation Technologies, India). For optical microscopy, test samples were smoothened with different emery papers up to 2000 grit size, followed by cloth polishing using the fine alumina particle suspension. After polishing, the samples were etched with a reagent containing a mixture of 1 % perchloric acid ($HClO_4$) and 99 % ethanol (C_2H_5OH).

The experiments were carried out on a pin-on-disc (Model TL- 40, Ducom India) to determine the sliding wear behavior of the AZ91D Mg alloy. Square cross-section pin-type samples of size 6 X 6 X 15 mm were cut, machined, and polished to conduct the test, as shown in Figure 1. These samples were also grounded with different emery papers (up to 2000 grit size), followed by cloth polishing. The polished sample surface roughness was maintained up to 0.2 μm before conducting the sliding wear tests in dry and SBF lubricated conditions. During the dry wear test, the flat square cross-section (6 X 6 mm) surface of the pin-type sample was kept in physical contact and pressed against a rotating corrosion-resistant stainless steel SS316L disc (95 HRB hardness) using different sliding speeds of 0.25, 0.5, and 1 m/s, normal loads of 20, 40, and 80 N and keeping the sliding distance to 2000 m.

Figure 1: Pin-type samples used in the wear testing.

Table 2: Details of chemicals with quantities for the SBF solution.

Reagents	**Amount**
Sodium sulfate (Na2SO4)	0.072 g
Potassium chloride (KCl)	0.225 g
Di-potassium hydrogen phosphate trihydrate (K2HPO4. 3H2O)	0.231 g
Calcium chloride (CaCl2)	0.292 g
Magnesium chloride hexahydrate (MgCl2.6H2O)	0.311 g
Sodium hydrogen carbonate (NaHCO3)	0.355 g
Tris-hydroxymethyl aminomethane ((HOCH2)3CNH2)	6.118 g
Sodium chloride (NaCl)	8.035 g
Hydrochloric Acid (1M-HCl)	39 ml
Hydrochloric Acid (1M-HCl)	0-5 ml

Using a digital weight measuring apparatus (Model N92, Essae-Troika, Japan) with an accuracy of 0.0001g, the sample's weight loss was measured before and after the experiment. Each experiment was performed three times to determine the average weight loss observed in three tests to ensure reproducibility. For conducting the wear tests in SBF solution conditions, a 1000 ml SBF solution was prepared using the different chemicals in calculated quantities, as given in Table 2, Kokubo and Takadama (2006).

For performing the wear test in the SBF solution, an additional arrangement was made in the existing pin-on-disc apparatus for containing the SBF solution over the disc surface, as shown in Figure 2. The volumetric wear rate formula was used to calculate the wear rate of the AZ91D alloy under various wear conditions (Ilanaganar and Anbuselvan, 2018) as shown in Equation (1).

$$Wr = \frac{m}{\rho L} \tag{1}$$

Wr, ρ, m, and L denote the volumetric wear rate, density, mass loss, and sliding distance respectively. The density of AZ91D alloy is considered to be 1.81 g/cm^3.

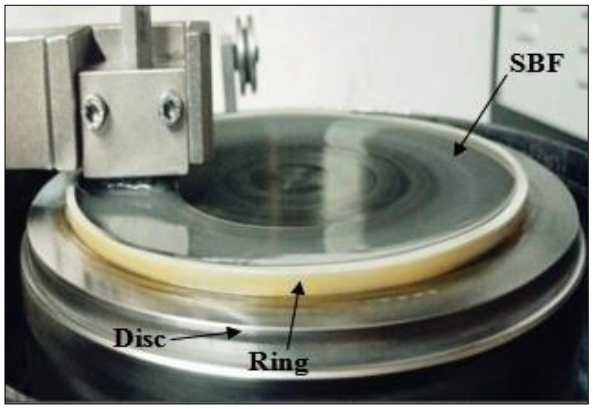

Figure 2: Wear testing under SBF solution.

2.0 RESULTS AND DISCUSSION

2.1 Microstructural and Microhardness Examination

SEM and OM images of AZ91D Mg alloy before the wear test are presented in Figures 3 (a and b), respectively. SEM was performed by using a 10 kV accelerating voltage at 250X magnification and 10 µm scale length. However, OM was performed at 200X magnification and 10 µm scale length. The β-phase is an aluminum-rich coarse eutectic phase, and it is distributed on the grain boundaries of the α-phase, as seen in Figure 3b. The average grain size of the samples was found to be approximately 10.18 µm. An EDS examination was also performed to confirm this material composition, as shown in Figure 4. The EDS report confirmed the presence of all significant elements closely matching the specifications of AZ91D material. Micro-hardness tests were performed using a micro-hardness tester (Make: Omnitech, India) at 10 sec dwell time and 100 g load. The micro-indents were observed at the surface on polished samples of the AZ91D material, and the average micro-hardness value was found to be 70±3 HV.

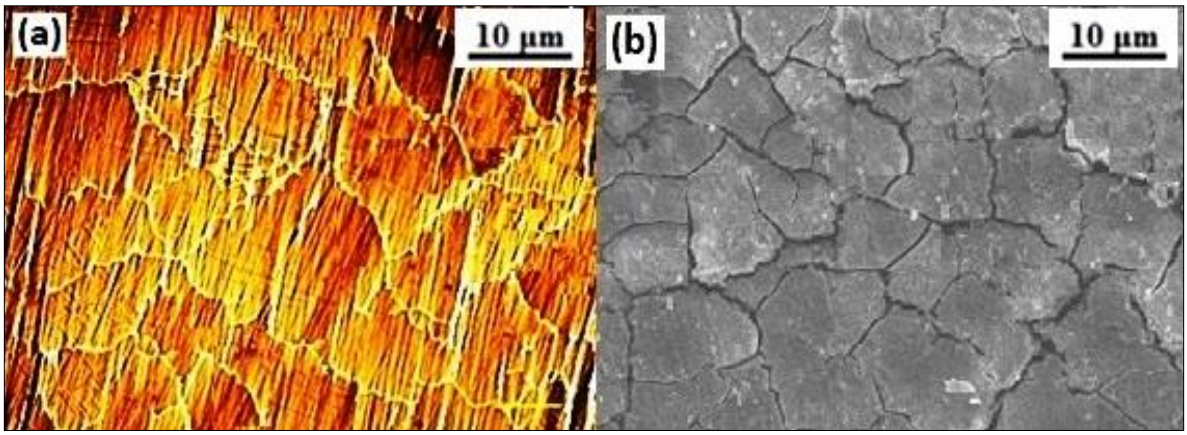

Figure 3: (a) Image from an optical microscope and (b) scanning electron microscopy showing the microstructure of AZ91D Mg alloy.

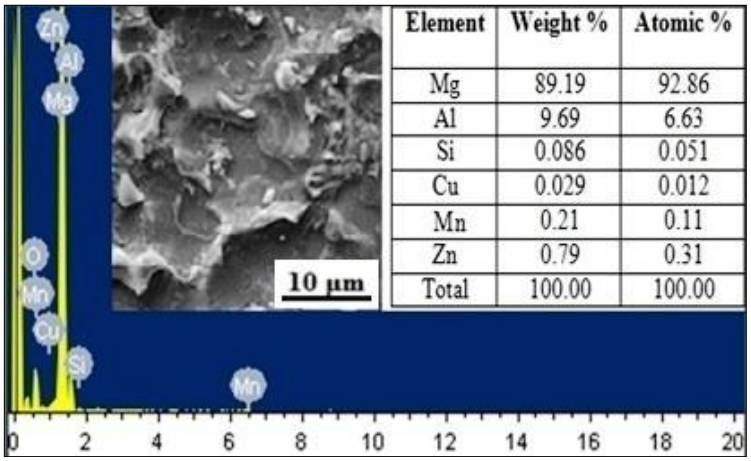

Element	Weight %	Atomic %
Mg	89.19	92.86
Al	9.69	6.63
Si	0.086	0.051
Cu	0.029	0.012
Mn	0.21	0.11
Zn	0.79	0.31
Total	100.00	100.00

Figure 4: EDX analysis of as-cast AZ91D material.

3.2 Wear Behavior

The volumetric wear rates of AZ91D Mg alloy versus loads applied at fixed sliding speeds (0.25, 0.5, and 1.0 m/s) in dry and SBF lubricated conditions are presented in Figure 5. At full sliding speeds, the wear rate is sharply rising with a rise in the applied load. A significant difference in wear rate is observed when the applied load was increased from 60 N to 80 N. The steep variation in the slope indicates the change from mild wear to severe wear regime (Chen and Alpas, 2000). Mild wear was maintained up to 40 N that is shown in the results. Moreover, increased wear rates were observed in SBF lubricated conditions compared to dry sliding. The volumetric wear rates of AZ91D Mg alloy versus sliding velocities used at fixed applied loads (20, 40, and 80 N) in dry and SBF conditions are given in Figure 6. The wear rate varies almost linearly along with the value of sliding velocity and applied loads. Although a significant change in wear rate slopes obtained when applied sliding speeds was 1.0 m/s. The result shows mild wear is controlled up to 0.5 m/s at 40 N load in dry condition, whereas up to 1.0 m/s at 40 N in the SBF solution condition for the investigated material.

It has been found that the AZ91D alloy develops viewable corrosion cavities when it is dipped in SBF, revealing some rapid corrosive wear. The corrosion attack occurs in the α-phase matrix mainly, and surface damage occurs due to pitting corrosion. Moreover, hollow indent develops from Cl^- and deep indent due to SO_4^-, and due to this, the Mg wear might occur. The MgO_2, $MgAl_2O_4$ and $MgAl_2(SO_4)4{\cdot}22H_2O$ are the main corrosion products, while the α-matrix and β-$Mg_{17}Al_{12}$ phases disappeared due to corrosion (Liying et al., 2018). The wear rate was increased in SBF solution compared to dry because of the presence of reactive SBF solution causing rapid corrosion, leading to the improvement in a mass loss under high loads at the warm surface of the AZ91D alloy during wear tests. The AZ91D alloy is not resistant to high wear rates, especially when there is an increment of contact temperature above 74˚C (Chen and Alpas, 2000). The surface temperature rises beyond 100˚C at an average load of 40 N, and severe wear rate results due to the disintegration and softening of the β phase in AZ91D alloy (Zafari et al., 2012).

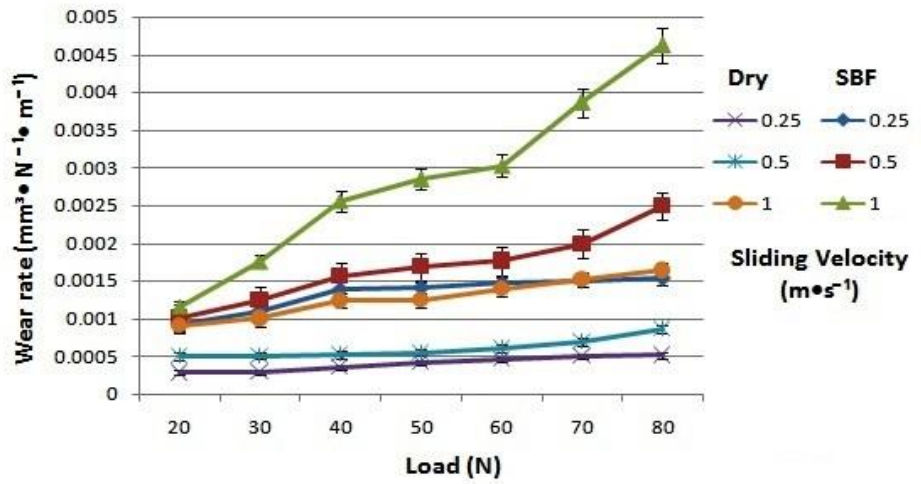

Figure 5: Effect of applied load at fixed sliding velocity on the wear rate in dry and SBF solution.

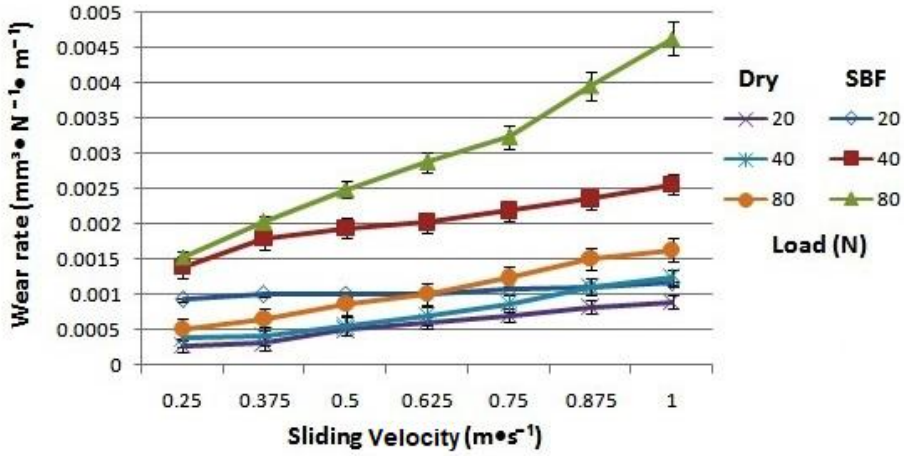

Figure 6: Effect of sliding velocity at fixed applied load on the wear rate in dry and SBF solution.

In this study, the tested pins worn out surfaces were observed to analyze the important wear mechanisms by EDS and SEM in specific wear conditions. Abrasive wear took place over the surface of samples at 0.25 m/s and 20 N in dry sliding conditions and 0.5 m/s and 20 N in SBF lubrication, respectively. It can be learned that the value of sliding velocity is more to induce abrasive wear in SBF than dry condition. The abrasive wear mechanism took place at a higher value of sliding velocity because of the SBF solution, which works as a lubricant. Abrasive wear of the investigated alloy after sliding wear tests in dry and SBF solution are shown in Figures 7 (a and b). Material has been removed due to the micro-cutting and micro-ploughing, leaving the displaced material and shear lips at the edges of wear tracks. These observations are in agreement with the previous findings (Ilanaganar and Anbuselvan, 2018).

Oxidation also plays out a noteworthy part in the wear behavior of the worn-out surface of metallic materials. A strong tendency of oxidation was found in the AZ91D Mg alloy. EDS scanning was carried out to determine the oxides formed on the worn-out sample surfaces in both test

conditions. Corrosive wear occurred in the samples at 0.5 m/s and 20 N in dry and SBF solution, respectively, as represented in Figures 8 (a and b). As per the SEM analysis, the dull surfaces are mainly shielded by a thin fine particle layer of MgO. The EDS patterns that appeared in Figures 9 (a and b) showed a definite oxygen peak in the spectrum, along with the peak of Mg.

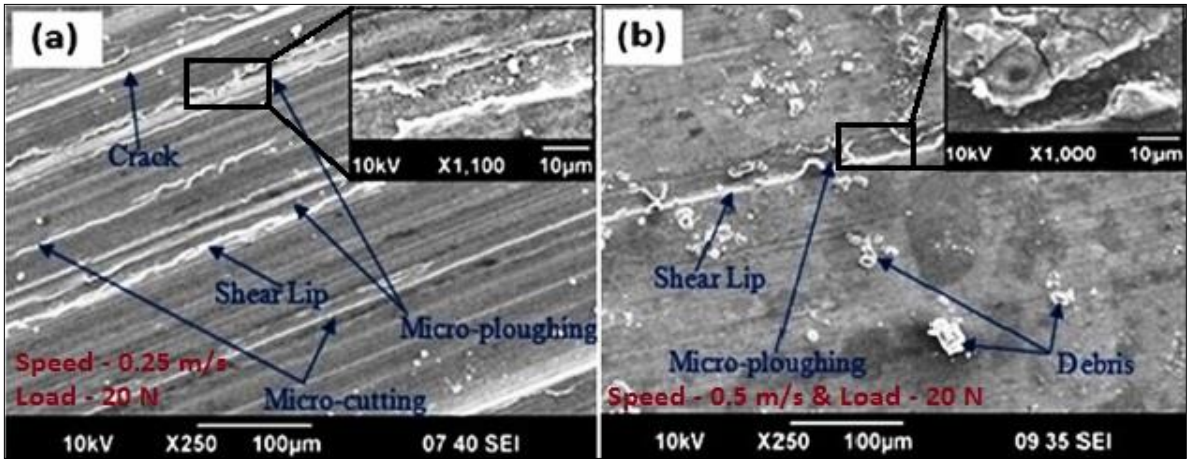

Figure 7: SEM images showing the scratches and grooves on pin surface in (a) dry and (b) SBF solution.

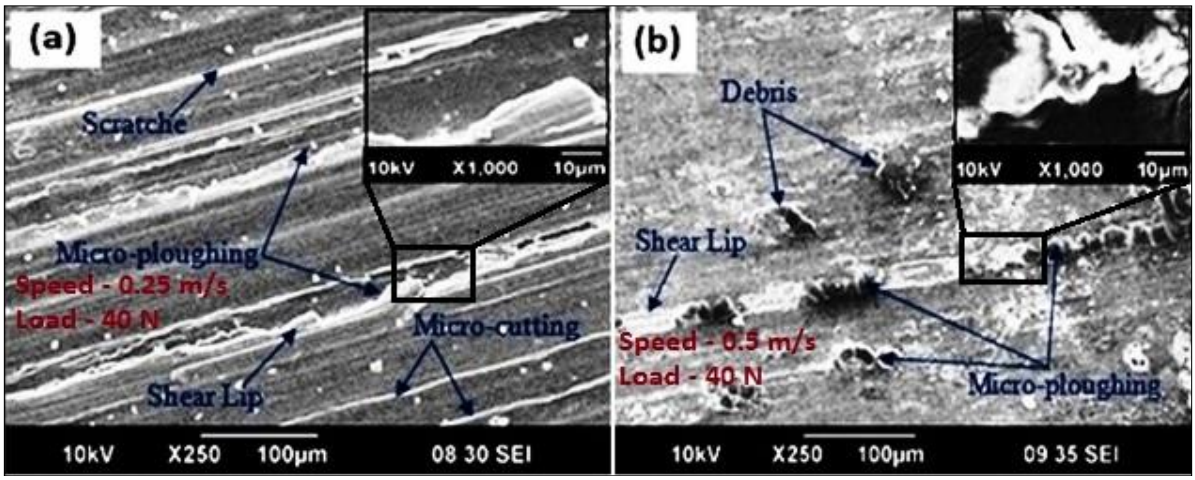

Figure 8: Image of SEM showing oxidation on pin surface in (a) dry and (b) SBF solution.

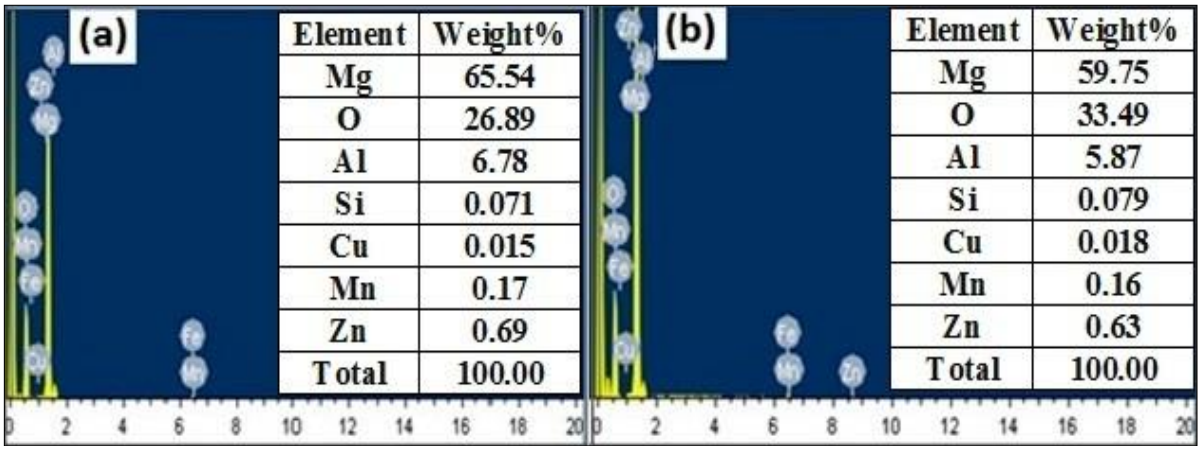

Figure 9: EDX analysis exhibiting firm oxygen peaks on the pin surface in (a) dry and (b) SBF solution.

Moreover, a stronger oxygen peak in the tested specimen represents greater oxidation in SBF solution (Figure 9b). The oxidation wear mechanism prevailed due to the frictional heat generation during the sliding motion and high affinity of Magnesium to atmospheric oxygen (in dry condition) and accelerated chemical reactions (in SBF solution) (Vignesh et al., 2020). Oxide wear crack fills the groove on the test surface because of the continued sliding motion, and it becomes set into a defensive layer. The base metal absolute wear rates took place because of the metallic contact between the rotating plate and test specimen. Chiranth et al. (2019) found that mild wear is accompanied by a low wear rate because of the oxide layer formation, which effectively secures the sliding surface of the material.

Figures 10 (a and b) represent SEM images, which show the delamination wear for samples at 0.5 m/s and 40 N in dry condition and at 1.0 m/s and 40 N in SBF solution, respectively. During the delamination, wear generally initiates from the short cracks, which appear coarsely opposite the sliding direction. The sizes of crack voids were 20-70 μm in length (Figure 10b). In the mild wear system, the materials wear behavior changes from oxidational to delamination wear when increasing the value of applied load (Ilanaganar and Anbuselvan, 2018) that can be seen in the case of dry sliding, but in the case of SBF, the value of both sliding speed and applied load is increased. The worn-out surface at lower loads identifies the significant hardening because the Mg alloy has low cold ductility (Xiao et al., 2018). As shown in Figures 11 (a and b), the EDS investigation shows that when the loose particles of the newly formed surfaces contact the air, the surface is slightly oxidized. Similarly, observation has been found in previous studies about wear in dry conditions (Lim, 2002).

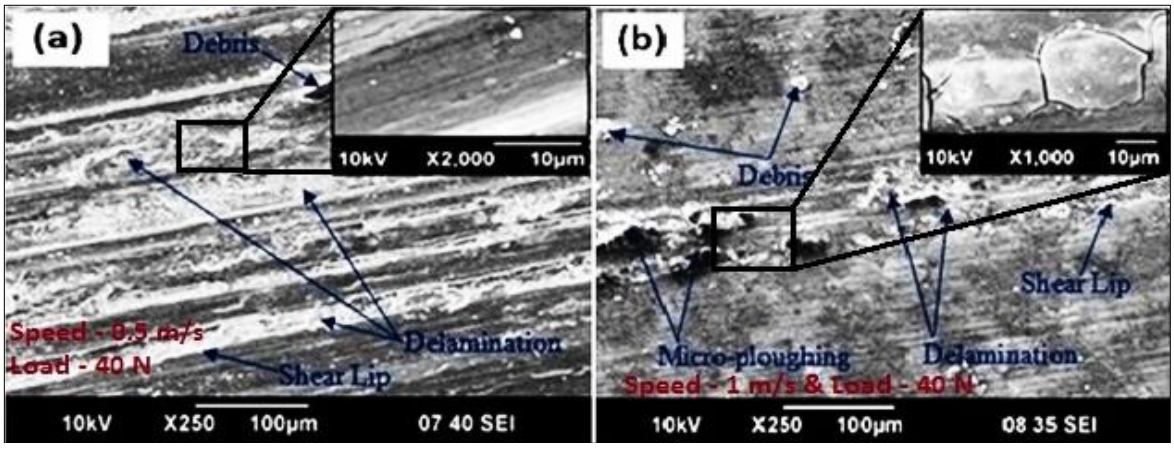

Figure 10: Image of SEM show cracks of pin surface show delamination in (a) dry and (b) SBF solution.

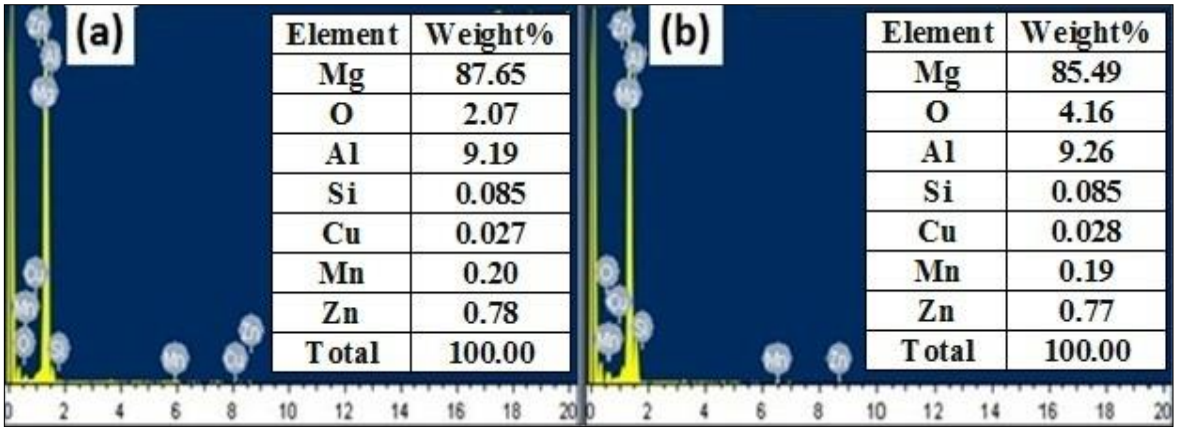

Element	Weight%
Mg	87.65
O	2.07
Al	9.19
Si	0.085
Cu	0.027
Mn	0.20
Zn	0.78
Total	100.00

Element	Weight%
Mg	85.49
O	4.16
Al	9.26
Si	0.085
Cu	0.028
Mn	0.19
Zn	0.77
Total	100.00

Figure 11: EDX analysis exhibiting low oxygen peaks on the pin surface in (a) dry and (b) SBF solution.

Plastic deformation has occurred in the worn-out surfaces of the samples at 40 N and 1.0 m/s in dry condition while at 80 N and 1.0 m/s in SBF solution, respectively, as shown in Figures 12 (a and b). Plastic deformation was identified on the work surface by immense surface damage without fracture. It can be clearly shown that the value of sliding velocity and applied load has been increased from the last mechanism, and an increase in speed and load leads to a higher wear rate, which introduces extensive surface damage to the investigated alloy in the form of plastic deformation (Mondal et al., 2007). The applied load value is more in SBF than dry due to more wear resistance at the same applied load value. The softening effect occurs on the material's surface due to frictional heating, which changes the wear from mild to severe form (Sun et al., 2018). As the temperature builds up due to immense frictional heat generated, alloy's strength diminishes proportionately, and easy plastic deformation becomes susceptible in the direction of sliding, leading to sideways spread of the worn-out surface (Mondal et al., 2007). In the wear test, sliding velocity and applied load have increased so much to cause the high frictional heat generation, which leads to thermal softening followed by the severe plastic flow of alloy under

investigation. It appeared to be like the melting of surface material in the localized region. A similar type of observation has been found in the case of AZ91 Mg alloy (Chen et al., 2018). Figures 13 (a and b) represent the SEM images of samples that have undergone thermal softening at 80 N and 1.0 m/s in dry and SBF lubrication. When the value of the applied load is increased above 60 N, then AZ91D alloy suffers from surface softening and plastic flow in dry conditions. However, in the SBF solution, this value of applied loads was 80 N and above. The worn-out material from the surface has flown plastically sideways along the sliding direction, and due to this generally thin layer formed in the solidified material. The new layers were repeatedly developed over the previous layers.

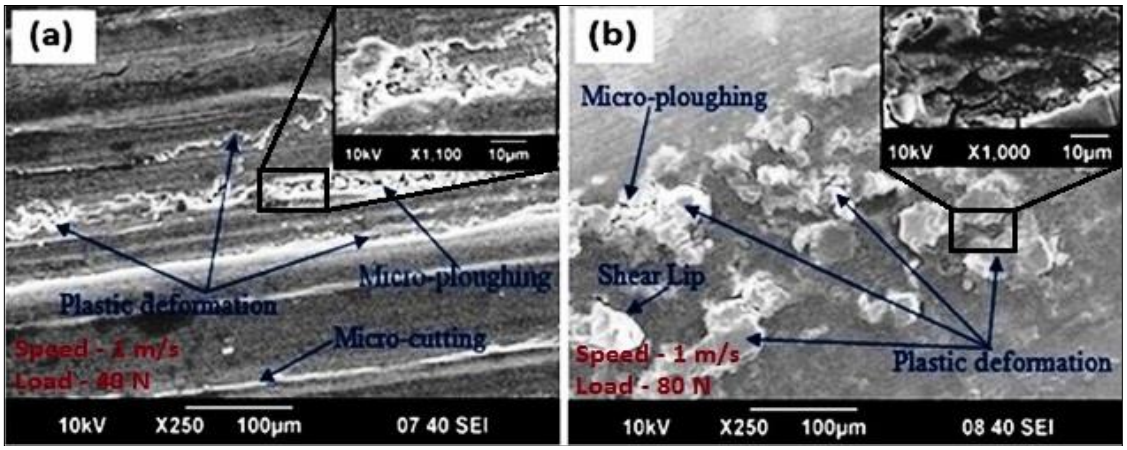

Figure 12: Image of SEM showing cracks on pin surface and plastic deformation in (a) dry and (b) SBF solution.

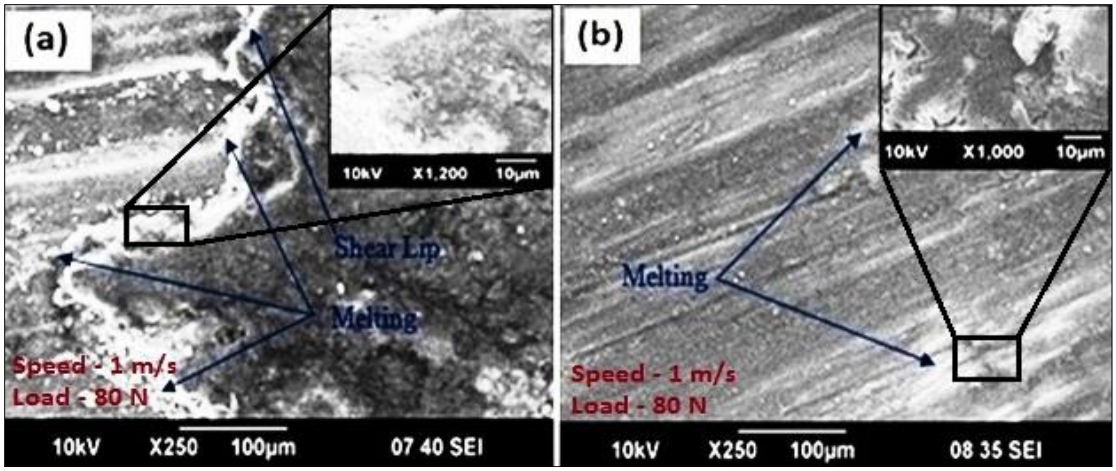

Figure 13: Image of SEM showing cracks on pin surface, indicating melting in (a) dry and (b) SBF solution.

2.3 Wear Map

Wear maps have been drawn to explain the AZ91D Mg alloy's wear behavior under different testing conditions. The investigated alloy's wear rate maps under dry sliding and SBF lubrication are presented in Figure 14 (a and b). The maps were made using the Origin software, representing the contours of volumetric wear rate data obtained for applied loads versus sliding speed. At a higher value of load and sliding speed, the wear rate is most extreme, and at a lower value of load and sliding speed, the wear rate is least for the investigated alloy (Krishnan et al., 2020).

The wear mechanism map is very much helpful to explain the behavior of the material under varying tribological conditions. A progress line that is an action of at least two proceeding parameters separates these map regions. Generally, lack of curvature and equal spacing lines means the same dominant mechanism is found in these maps. By evaluating the regions, the distinctive wear mechanisms can be characterized. To calculate the different wear conditions, wear maps could be useful (Lim, 2002). In SBF lubrication, the value of the load or sliding speed is more than dry conditions for switching into a more severe form of wear. However, the wear rate was increased in SBF solution than dry because of rapid corrosion of the alloy (Liying et al., 2018). On the other hand, SBF worked as a lubricant that did not allow the mechanism to change at the same sliding speed and applied load value compared to dry conditions.

The main wear regimes for AZ91D Mg alloy are mild wear, severe wear, and ultra-severe wear. In the mild wear regime, abrasion, delamination, and oxidation wear occur for the investigated alloy. However, the removal of material in the severe wear regime is the mechanism of severe plastic deformation. On the other hand, in the ultra-severe wear regime, the material's thermal softening and plastic flow are observed. A mild wear regime could be selected for any applications or safe operation, as the wear rates are generally low in this regime. Figures 15 (a and b) presented the wear regimes for AZ91D Mg alloy in dry and SBF solution, respectively.

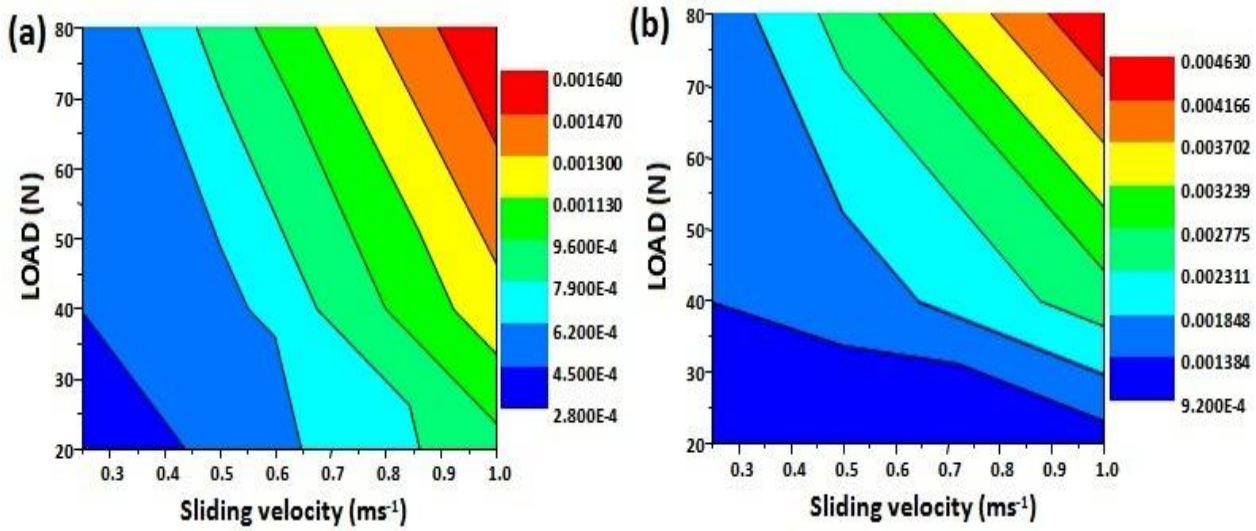

Figure 14: Wear rate map of AZ91D Mg alloy in (a) dry (b) SBF solution.

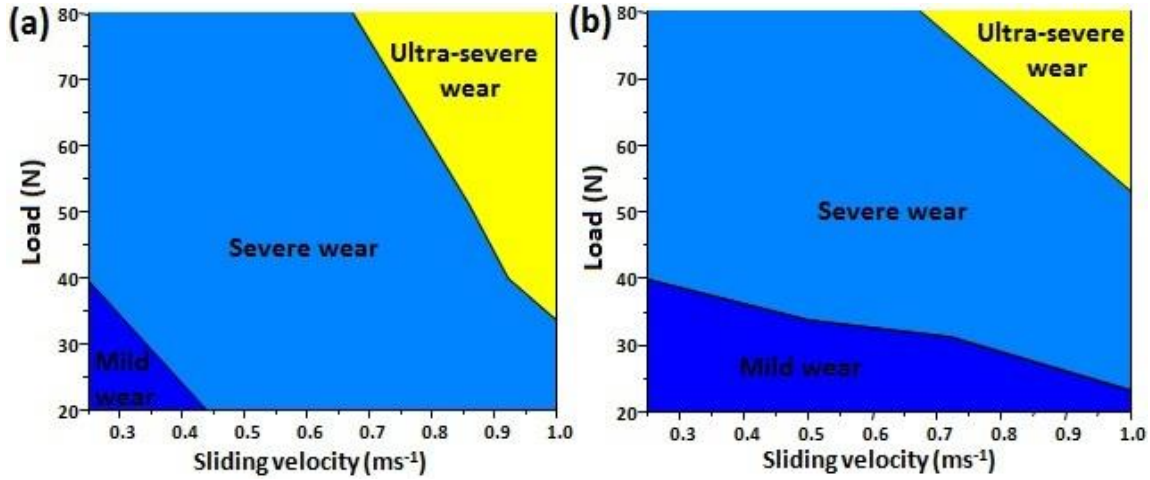

Figure 15: Wear mechanism maps of AZ91D Mg alloy in (a) dry (b) SBF solution.

CONCLUSIONS

This article will help in further study of AZ91D Mg-based materials for the recent trends in the emerging area for bio-implants. An enhancement in the wear rate was found on raising the value of applied loads and sliding speeds for AZ91D Mg alloy in dry and SBF solution. The following conclusions can be made in this research:

(a) An enhancement in the alloy's wear rate was observed to increase the sliding speed values and applied load in dry and SBF solution.
(b) In SBF lubrication, the sliding velocity and load values are greater than the value of load and sliding velocity in dry conditions for switching into a more severe form of wear.
(c) SBF worked as a lubricant that did not allow the mechanism to change at the same sliding speed and applied load value compared to dry conditions.
(d) The wear rate was increased in SBF reactive solution than dry sliding because of the rapid corrosion of alloy.
(e) Wear maps are useful in defining the wear regimes and wear behavior of AZ91D alloy in dry and lubricated tribological conditions.
(f) The important wear mechanisms in mild wear are abrasion, delamination, and oxidation. Plastic deformation is observed in the severe wear regime, while in the ultra-severe wear regime the thermal softening followed by severe plastic flow is the dominant wear mechanism. All three wear regimes were observed in both dry and SBF lubricated tribological conditions.

REFERENCES

Chelliah, N. M., Kumar, R., Singh, H., & Surappa, M. K. (2017). Microstructural evolution of die-cast and homogenized AZ91 Mg-alloys during dry sliding condition Journal of Magnesium and Alloys, 5, 35-40.

Chen, H., & Alpas, A. T. (2000). Sliding wear map for the magnesium alloy Mg-9Al-0.9 Zn (AZ91). Wear, 246, 106-116.

Chen, Q., Zhao, Z., Zhu, Q., Wang G., & Tao, K. (2018). Cerium Addition Improved the Dry Sliding Wear Resistance of Surface Welding AZ91 Alloy. Materials,11, 250.

Chen, Y., Dou, J., Yu, H., & Chen, C. (2019). Degradable magnesium-based alloys for biomedical applications: The role of critical alloying elements. Journal of Biomaterials Applications, 33, 1348-1372.

Chiranth, B.P., Siddaraju, C., Mishra, R.K., Sasikumar, R., Sathiskumar, R., & Prabhu, T. (2019). High-Temperature Wear Behavior of the ZE41 Mg Alloy. Materials Science Forum, 969, 86-92.

Ilanaganar, E., & Anbuselvan, S. (2018). Wear mechanisms of AZ31B magnesium alloy during dry sliding condition. Materials Today: Proceedings, 5, 628–635.

Imran, M., & Lathe, R. M. (2018). Synthesis and wear behaviour of mg az91d magnesium alloy reinforced with silicon carbide (sic) and graphite (gr) particulates. International Journal of Technical Innovation in Modern Engineering & Science, 4, 660-670.

Kang, M., Lee, H., Jang, T., Seong, Y., Kim, H., Koh, Y., Song, J., & Jung, H. (2019). Biomimetic porous Mg with tunable mechanical properties and biodegradation rates for bone regeneration. Acta Biomaterialia, 84, 453-467.

Kokubo, T., & Takadama, H. (2006). How useful are SBF in predicting in vivo bone bioactivity. Biomaterials, 27, 2907-2915.

Kong, X., Wang, L., Li, G., Qu, X., Niu, J., Tang, T., Dai, K., Yuan, G., & Hao, Y. (2018). Mg-based bone implants show promising osteoinductivity and controllable degradation: A long-term study in a goat femoral condyle fracture model. Materials Science & Engineering C, 86, 42-47.

Krishnan, C., Pokhrel, R., Mondal, A. K., & Masanta, M. (2020). Effect of temperature and applied load on sliding wear behaviour of AZ91D magnesium alloy. Materials Today: Proceedings, 26, 1136-1139.

Kumar, D., Jain, J., & Gosvami, N. N. (2020). In-situ study of role of microstructure on antiwear tribofilm formation on AZ91 magnesium alloy under ZDDP containing lubricant. Advanced Engineering Materials, 22, 202000335.

Kumar, S., Jain, J., & Kumar, D. (2017). Tribological Study of Heat Treated AZ91 Alloy against Al6351 under Dry Conditions. Key Engineering Material, 737, 168-173.

Li, H., Liu, D. B., Zhao, Y., Jin, F., & Chen, M. F. (2016). The influence of Zn Content on the corrosion and wear performance of Mg-Zn-Ca Alloy in Simulated Body Fluid. Journal of Materials Engineering and Performance, 25, 3890-3895.

Lim, S.C. (2002). The relevance of wear-mechanism maps to mild-oxidational wear. Tribology International, 35, 717-723.

Liying, C., Zhiyong, L., Peng, H., Jiamin, S., Xiaogang, L., Cuiwei, D., & Bin, J. (2018). The Corrosion Behavior of AZ91D Magnesium Alloyin Simulated Haze Aqueous Solution. Materials, 11, 970-988.

Makkar, P., Sarkar, S., Padalhin, A. R., Moon, B., Lee, Y., & Lee, Y. (2018). In vitro and in vivo assessment of biomedical Mg–Ca alloys for bone implant applications. Journal of Applied Biomaterials & Functional Materials, 16, 126-136.

Mondal, A.K., Chandra Rao, B.S.S., & Kumar, S. (2007). Wear behavior of AE42+20% safe Mg MMC. Tribology International, 40, 290-296.

Peron, M., Torgersen, J., & Berto, F. (2017). Mg and its alloys for biomedical applications: exploring corrosion and its interplay with mechanical failure. Metals, 7, 252-293.

Radha, R., & Sreekanth, D. (2017). Insight of magnesium alloys and composites for orthopedic implant applications – a review. Journal of Magnesium and Alloys, 5, 286-312.

Ratna Sunil, B., Ganesh, K. V., Pavan, P., Vadapalli, G., Swarnalatha, Ch. P., & Swapna Bindukumar, P. (2016). Effect of aluminum content on machining characteristics of AZ31 and AZ91 magnesium alloys during drilling. Journal of Magnesium and Alloys, 4, 15-21.

Sathish, S., Anandakrishnan, V., Sankaranarayanan, S., & Gupta, M. (2019). Optimization of wear parameters of magnesium metal-metal composite using Taguchi and GA technique. Jurnal Tribologi, 23, 76-89.

Siti, R. M., Saiful, A. C., & Ghani, W. S. (2019). Mechanical properties of additive manufactured CoCrMo meta-biomaterials for load bearing implants. Jurnal Tribologi, 21, 93-107.

Staiger, M., Pietak, A., Huadmai, J., & Dias, G. (2006). Magnesium and its alloys as orthopedic biomaterials: A review. Biomaterials, 27, 1728-1734.

Sun, W., Xuan, X., Li, L., & An, J. (2018). Tribological Behavior and the Mild–Severe Wear Transition of Mg97Zn1Y2 Alloy with a LPSO Structure Phase. Materials, 11, 1-20.

Vignesh, R., Padmanaban, R., & Govindaraju, M. (2020). Study on the corrosion and wear characteristics of magnesium alloy AZ91D in simulated body fluids. Bulletin of Materials Science, 43, 1-12.

Xiao, P., Gao, Y., Xu, F., Yang, C., Li, Y., Liu, Z., & Zheng, Q. (2018). Tribological behavior of in-situ nanosized TiB2 particles reinforced AZ91 matrix composite. Tribology International, 128, 130-139.

Xiaobo, Z., Jianwai, D., & Yunqiang, B. (2019). Quantative Evaluation of the Interaction between Wear and Corrosion on Mg-3Gd-1Zn Alloy in Simulated Body Fluid. Journal of Materials Engineering and Performance, 28, 355-362.

Zafari, A., Ghasemi, H. M., & Mahmudi, R. (2012). Tribological behavior of AZ91D magnesium alloy at elevated temperatures. Wear, 292, 33-40.

Zhou, X., LI, Li., Wen, D., Liu, X., & Wu, C. (2018). Effect of hybrid ratio on friction and wear behavior of AZ91D matrix nanocomposites under oil-lubricated conditions. Trans. Nonferrous Met. Soc. China, 28, 440−450.